

PAPER • OPEN ACCESS

Effect of repeated TIG welding cycles on microstructure evolution and pitting corrosion behavior of UNS 32760 super duplex stainless steel

To cite this article: Alfian *et al* 2019 *IOP Conf. Ser.: Mater. Sci. Eng.* **478** 012032

View the [article online](#) for updates and enhancements.

Effect of repeated TIG welding cycles on microstructure evolution and pitting corrosion behavior of UNS 32760 super duplex stainless steel

Alfian, R Riastuti, and Winarto

Department of Metallurgy and Materials Engineering, Faculty of Engineering, University of Indonesia

Email: alfianzero@gmail.com

Abstract. Microstructure evolution and pitting corrosion behavior in repeated TIG welding cycles of UNS32760 super duplex stainless steel were studied. The microstructural evolution was observed through optical electron microscope. Meanwhile, pitting corrosion was investigated by means of potentiodynamic polarization and gravimetric test. The specimens were evaluated to simulate repeated welding cycles of original weld, Repair-1 (R1), Repair-2 (R2) and Repair-3 (R3) respectively. The result shows that the chromium nitride precipitates start to appear in the heat-affected zone R-2 welding cycles which followed by the growth of metastable pits.

1. Introduction

Super Duplex Stainless Steel (SDSS) is a material that is formed by a unique combination of ferrite and austenite microstructure that ideally has the same large volume fraction that offers an interesting combination of mechanical properties and corrosion resistance [1,3]. These excellent properties depend on its chemical composition (Cr, Mo, N and Ni) and the right balance between ferrite (α) and austenite phases (γ) [4]. Therefore, SDSS is widely used in the oil, chemical, petrochemical, nuclear and marine industries because of its attractive combination of mechanical strength and higher corrosion resistance in a variety of aggressive environments [2,5]. GTAW is the most common type of welding used in DSS and SDSS materials in various industries [1]. Rapid heating and cooling cycles in the welding process can interfere with the α / γ phase balance and result in precipitation of intermetallic phases such as sigma, chi, secondary austenite and chromium nitride. These can reduce mechanical properties and corrosion resistance of super duplex stainless steel materials [1,2,4].

Many studies have been carried out related to changes in microstructure due to the welding process in SDSS materials which have an impact on mechanical properties and corrosion resistance, but studies and references in repeated welding cycles of SDSS materials are very rare. Some information obtained from several standards / codes such as the NORSOK M-601 clause 7 only allows for one weld repair on SDS material. DNV-OS-F101 Table C-7 Appendix C, prohibits repetition of welding repairs to SDSS material



[6]. In fact, because of the difficulty in obtaining quality welds of SDSS material, repaired welding are often carried out. The present study investigated the effect of heat cycles on microstructure evolution and pitting corrosion behavior of UNS 32760 repeated welds. The TIG welding process was executed on 2" sch. 160 pipes with 6G welding position and carried out with appropriate welding parameters.

2. Methodology

2.1. Material and welding process

The base material employed is a commercial UNS 32760 SDSS produced by Tubacex Tubos Inoxidables. The alloy has been solution annealed and quenched by water into 2" pipe of about 8.74 mm thickness. The chemical compositions of base metal and filler are shown in Table 1. The pipes were butt-welded with TIG welding. The welding parameters are listed in table 2. Welding is employed by GTAW with DC-EN polarity and 6G position. The backing and shielding gas used are Ar + 2% N. Test coupons are prepared as shown in Figure 1 and given a datum mark or line 60 mm from the edge of the bevel area as a reference line in cutting and preparing samples for the repair process. In the R-1 sample preparation, the OW sample was cut and machined to form a bevel on the same fusion line area as OW with reference to the datum line to keep the heat-affected zone the same. The beveling process for R-2 and R-3 sample applied the same.

Table 1. Chemical compositions of base metal and filler

Element (%)	C	Si	Mn	P	S	Cr	Mo	Ni	Cu	W	N	Al	PREN
Base Metal	0.02	0.5	0.7	0.02	0.001	25.7	3.7	7.00	0.7	0.6	0.27	-	42.02
Filler	0.01	0.5	0.5	0.02	0.001	25.1	3.9	9.2	0.1	0	0.27	0.01	42.1

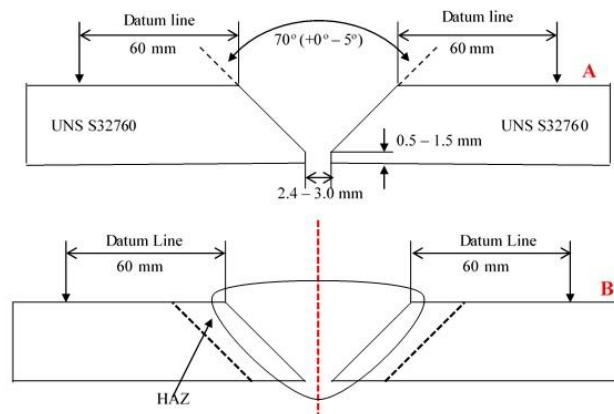


Figure 1. Joint Design: (A) Preparation and fit up of welding test coupons, (B) Cutting scheme of repaired test coupons.

Table 2. Welding Parameter

Joint Design	Welding current (A)	Welding voltage (V)	Welding speed (mm/min)	Shielding gas flow: Ar (L/min)	Backing gas flow: Ar (L/min)
Single V Groove	60 - 78	10	21.52 - 83.12	10 - 20	5 - 15

2.2. Microstructure characterization

To observe the optical micrographs of the WM, HAZ, and BM, the specimens were polished with silicon carbide up to 1000 grit followed by a cloth polishing with 0.05 μ m alumina powder and etched in 30% NaOH electrolyte [7]. The volume fraction of the ferrite and austenite phases was evaluated carefully by means of a BX53M Olympus optical microscope.

2.3. Corrosion and Electrochemical Measurements

Gravimetric test were conducted at 22°C for 72 h in the ferric chloride solution according to ASTM G48 Method A. The specimen dimension is 25 by 50 mm (1 by 2 in.) with 10mm Thickness. The solution was prepared by dissolving 100 gram of FeCl₃.6H₂O in 900 mL of deionized water with constant pH. After the soaking time, the specimens were rinsed with water and brushed with nylon to remove corrosion products then dipped in acetone and left to dry at room temperature. The weight losses of the specimens were recorded [8, 9]. Electrochemical Measurement were carried out with a GAMRY Reference 600+ in a three-electrode cell held in a water bath. The counter electrode was a platinum foil, and the saturated calomel electrodes (SCE) were used as the reference electrode. All potentials were given against the SCE. The test solution, 1 mol/L NaCl, was made by dissolving 58.45 g of NaCl in water until the solution mixture reaches a volume of 1L. The working electrodes were mounted in epoxy resin. The specimens were passivated with 20% nitric acid (HNO₃) at ambient temperature for 1 h to avoid crevice corrosion in specimen/resin interfaces then abraded with 600 grit paper. The minimum test area is 1 cm². The potentiodynamic polarization tests were conducted at a scanning rate of 1 mV/s from -0.7 V to a very anodic potential at 23°C \pm 2°C. The potential at which the current density exceeded 100 μ A/cm² is defined as pitting potential. Before corrosion and electrochemical tests were conducted, the specimens have been polished with silicon carbide up to 1000 grit [10-13].

3. Result and discussion

3.1. Microstructure Evolution

Fig. 2a shows microstructure of the base metal. The light area is austenite while the dark is ferrite. Ferrite and austenite phases extend and assemble along the direction of the material plane with the same volume fraction. There are no precipitates in both ferrite and austenite. This indicates the volume balance of the ferrite and austenite phases. The appearance of microstructure at the base material is the same for all weld repairs.

Fig. 2b exhibits how the heat cycle in the welding process destroys the balance of ferrite and austenite phases. In this zone there are several types of austenite: Grain boundary austenite (GBA), Widmānsttenaustenite (WA), intra-granular austenite (IGA) and secondary austenite (γ_2). During the welding process, GBA is formed on the ferrite grain boundary because there is a large amount of free energy at this location. WA continues to form and grow around GBA. At the same time IGA and secondary austenite are formed in this zone because there are many nickel elements as austenite stabilizers carried by filler metals [4]. It can also be seen that GBA is coarser compared to WA and IGA. This indicates instability in the ferrite and austenite interfaces [2].

In Fig. 2c, the GBA is clearly visible with a thinner and smoother structure with a small amount of IGA. In this zone the ferrite volume fraction is far more compared to austenite. This is due to the high temperature of welding [2]. Fig. 2d has almost the same structure as fig. 2c with GBA is more coarse and thicker and relatively more austenite volume fractions characterized by more IGA.

Fig. 2e is the HAZ R-2 microstructure. R-2 HAZ is relatively narrow compared to OW and R-1 so that the structure is not clearly visible. The narrow HAZ as a transition area is strongly influenced by both BM and WM structures with a higher volume of austenite fraction compared to ferrite. In this condition, the chromium nitride (Cr_2N) precipitate which is marked by black spot on the ferrite grains appeared.

Fig. 2f shows the HAZ which is slightly wider than fig. 2e more ferrite volume fractions. GBA looks clearer with a combination of fine/thin and thick/rough types and there are more chromium nitride precipitates.

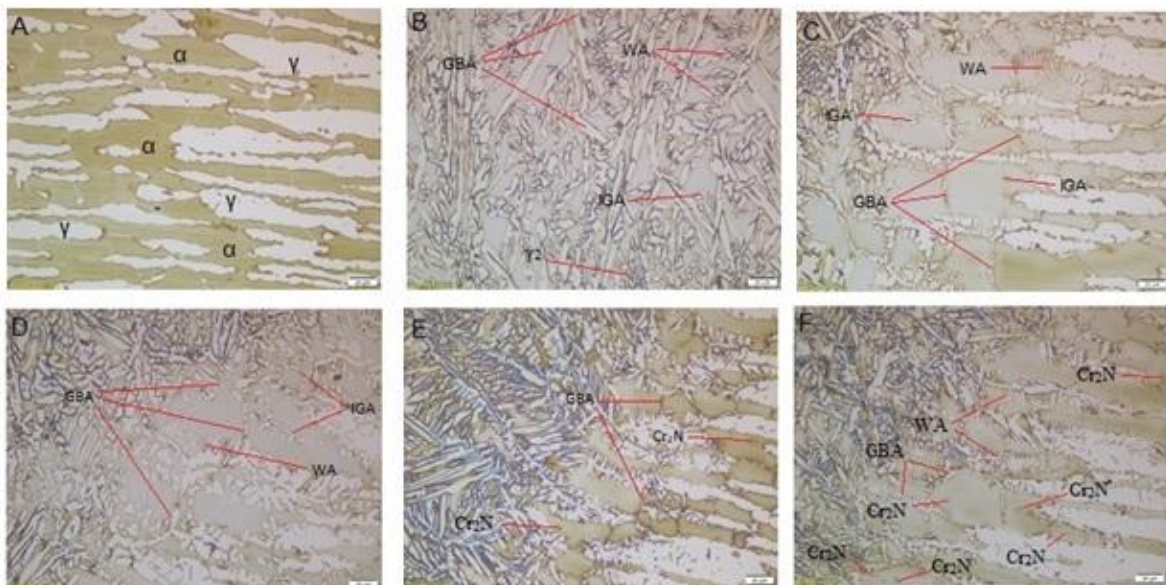


Figure 2. Optical microstructure of BM, HAZ and WM of repeated TIG welding: (a) base metal, (b) weld metal, (c) HAZ for OW, (d) HAZ for R-1, (e) HAZ for R-2, (f) HAZ for R-3.

3.2. Pitting Corrosion Resistance

Gravimetric Test and Potentiodynamic anodic polarization technique were used to evaluate the effect of repeated TIG welding cycles on the pitting corrosion resistance of the test specimens. The results of the gravimetric tests are listed in table 3. It is obvious that R-3 welding cycles has highest corrosion rate during the test followed by R-2, OW and R-1. The anodic polarization curves are presented in Fig. 3. The polarization pattern on all specimens is relatively the same where the specimen is passivated before the occurrence of pitting. The R-3 has the largest passive current density followed by R-2, OW and R-1. The appearance of the current peaks triggered under E_{pitt} in R-2 showed that the specimen was attacked by metastable pits [2] as shown in figure 4. The current density magnitude of the specimens showed that the R-3 has the highest corrosion rate during the measurement. The results of the polarization measurements are listed in table 4. The open circuit potential (OCP) value starts with negative value, continuously increase to positive and decrease to more negative. Thermodynamically, the more negative the OCP, the higher tendency the corrosion takes place [4, 12]. As well as OCP, E_{corr} starts with negative values,

increase to positive and back to negative. The value of E_{pitt} showed significantly decrease by increasing the number of repeated welding cycles. Taking both corrosion rate and anodic polarization into consideration, it can be concluded that R-3 has the poorest pitting corrosion resistance followed by R-2.

Table 3. Gravimetric Test Result of repeated TIG welding

No	Specimen	Area (cm ²)	Weight before test (g)	Weight after test (g)	Weight loss (g/cm ²)	Corrosion Rate (mdd)
1	OW	33.7408	49.0500	49.0483	0.00005	1,68
2	R1	35.8517	53.2932	53.2914	0.00005	1,67
3	R2	32.9367	48.3204	48.3165	0.00012	3.95
4	R3	34.6789	48.4726	48.4454	0.00078	26,08

Table 4. Electrochemical parameters of therepeated TIG welding

No	Specimen	OCP (V vs SCE)	E _{corr} (V vs SCE)	E _{pitt} (V vs SCE)
1	OW	-0.222	-0.4559	0.7135
2	R1	0.1899	0.01792	0.7276
3	R2	0.009132	-0.3206	0.6869
4	R3	-0.2403	-0.394	0.6835

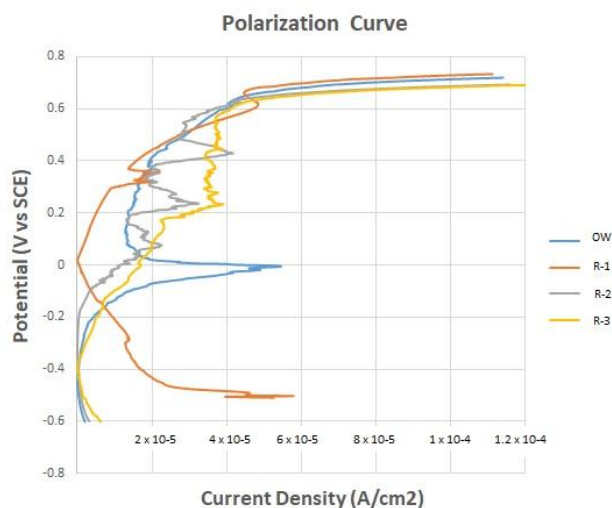


Figure 3. Polarization curves of repeated TIG welding

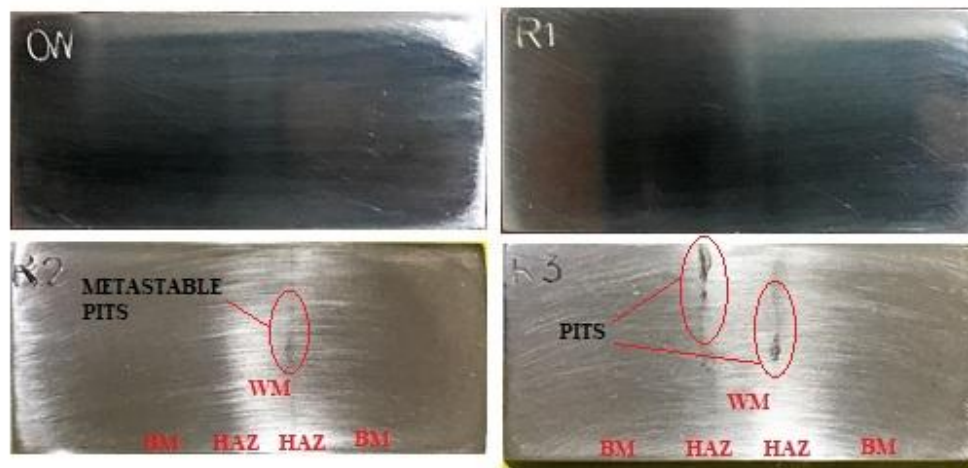


Figure 4. Specimens of repeated TIG welding after gravimetric tests

4. Conclusion

The effect of repeated TIG welding cycles on microstructure evolution and pitting corrosion behavior of UNS 32760 super-duplex stainless-steel were investigated by morphological observation and electrochemical measurements. The more repetition of welding cause the coarser grain growth, the more ferrite volume fraction and the more chromium nitride precipitates in heat-affected zone. The chromium nitride precipitates and the metastable pits start appearing in R-2 welding cycles and make the pitting corrosion resistance start to decrease.

References

- [1] Prabhu P and Rajnish G 2016 *Engineering Science and Technology, an International Journal* **19** 1076–1083
- [2] Ziying Z, Hui Z, Huizhen Z, Jun H, and Jiarui J 2017 *Corrosion Science* **121** 22–31
- [3] Hua T, Yiming J, Bo D, Tao S, Juliang X, Jin L 2009 *Material Characterization* **60** 1049-1054
- [4] Shaoning G, Junsheng S, Lingyu G, Hongquan W 2015 *Journal of Manufacturing Processes* **19** 32–37
- [5] Bo D, Zhiyu W, Yiming J, Hao W, Juan G, Jin L 2009 *Electrochimica Acta* **54** 2790–2794
- [6] Danny S M and Turnad L G 2016 *ARPN Journal of Engineering and Applied Sciences* **11** (14)
- [7] ASM International 2014 *Standard Practice for Microetching Metals and Alloys (ASTM E407)*
- [8] ASM International 2011 *Standard Test Methods for Pitting and Crevice Corrosion Resistance of Stainless Steels and Related Alloys by use of Ferric Chloride Solution (ASTM G48)*
- [9] Jyoti B, Samantha L, Rouzbeh A, Vikram G, Roberto O, Denis L, and Faisal K 2017 *Journal of Loss Prevention in the Process Industries* **47** 10-21
- [10] ASM International 2004 *Standard Reference Test Method for Making Potentiostatic and Potentiodynamic Anodic Polarization Measurements (ASTM G5)*
- [11] Alonso-Falleiros N, Hakim A, and Wolyne S 1999 *Corrosion* **5(5)** 443-448
- [12] Luo H, Dong C F, Cheng X Q, Xiao K, and Li X G 2011 *Journal of Materials Engineering and Performance*
- [13] Sun Y T, Wang J M, Jiang Y M, and Li J 2018 *Materials and Corrosion* **69** 44-52